INT. J. REMOTE SENSING, 10 DECEMBER, 2004,
VOL. 25, NO. 23, 5255–5266

Equator crossing times for NOAA, ERS and EOS sun-synchronous satellites

A. IGNATOV*, I. LASZLO

NOAA/NESDIS, Office of Research and Applications, E/RA1, Room 603, WWB, 5200 Auth Road, Camp Springs, MD 20746-4304, USA

E. D. HARROD

NOAA/NESDIS, Office of Satellite Data Processing and Distribution, E/SP13, FB4, Room 0318, 5200 Auth Road, Suitland, MD 20746-4304, USA

K. B. KIDWELL

NOAA/NESDIS, Office of Systems Development, E/OSD, Room 5126, SSMC1, 1335 East-West Highway, Silver Spring, MD 20910, USA

and G. P. GOODRUM

NOAA/NESDIS, Office of Systems Development, Polar Program Office, E/OSD, FB3, Room G229, 5200 Auth Road, Suitland, MD 20746-4304, USA

(*Received 31 July 2003; in final form 9 February 2004*)

Abstract. The local Equator Crossing Times (EXT) of the 13 National Oceanic and Atmospheric Administration (NOAA) platforms (TIROS-N and NOAA-6 through -17) flown from 1978 until the present have been summarized as a function of time and approximated analytically. The fit equations accurately reconstruct all past EXTs to within ± 2 min and also allow extrapolation in time, thus providing a useful insight into the phenomenology of its evolution. The EXTs of the three European Research Satellites (ERS: ERS1, ERS2 and Envisat) and two Earth Observing System satellites (EOS: Terra and Aqua) are also presented. In contrast to the NOAA platforms, the ERS/EOS orbits are adjusted in-flight. This makes an analytical fit to the resulting man-made EXTs impractical, and less needed as the EXTs are more stable.

1. Introduction

Since 1978, the TIROS-N (TN) (TIROS-N, NOAA-6, -7 and -12) and Advanced TIROS-N (ATN) (NOAA-8, -9, -10, -11, -13, -14, -15, -16, -17) series of National Oceanic and Atmospheric Administration (NOAA) polar orbiting satellites have become an indispensable source of unique global meteorological and climatological information about the Earth (e.g. Rao *et al.* 1990, Kidder and Vonder Haar 1995, Cracknell 1997, 2001). The NOAA satellites have been designed to be sun-synchronous, however, their orbits change in time. This 'orbital drift'

*Corresponding author; e-mail: Alex.Ignatov@noaa.gov

International Journal of Remote Sensing
ISSN 0143-1161 print/ISSN 1366-5901 online © 2004 Taylor & Francis Ltd
http://www.tandf.co.uk/journals
DOI: 10.1080/01431160410001712981

causes a platform to systematically progress through different phases of the solar illumination and diurnal cycle of the underlying surface and atmosphere, thus modulating radiances measured by every single instrument onboard NOAA platforms, and affecting meteorological and climate products derived therefrom. Numerous examples are found in the literature for the Advanced Very High Resolution Radiometer (AVHRR) (e.g. Price 1991, Gutman and Ignatov 1995, Privette *et al.* 1995, Brest *et al.* 1997, Gutman 1999 a,b, Kogan and Zhu 2001, Stowe *et al.* 2002, Cao *et al.* 2002, Reynolds and Gentemann 2004), for the TIROS Operational Vertical Sounder (TOVS, consists of three instruments: the High Resolution Infrared Radiation Sounder, HIRS, the Microwave Sounding Unit, MSU, and the Stratospheric Sounding Unit, SSU) (e.g. Brownscombe *et al.* 1985, Bates *et al.* 1996, Waliser and Zhou 1997, Jackson and Bates 2001, Christy *et al.* 2003, Mears *et al.* 2003, Menzel *et al.* 2002, Vinnikov and Grody 2003), and for the Solar Backscatter Ultraviolet Radiometer (SBUV) (e.g. Flynn *et al.* 2000, Miller *et al.* 2002).

The change in the local solar time (LT) of observation is closely tracked by the changes in LT when a platform crosses the equator (Equator Crossing Time, EXT). In some of the studies cited above, limited time series of the NOAA EXTs have been plotted for selected portions of active phases of some NOAA platforms. The orbits of the more recent European Research Satellites (ERS: ERS1, ERS2 and Envisat) and Earth Observing System satellites (EOS: Terra and Aqua) are corrected in-flight, which is supposed to maintain a constant EXT. However, their actual EXTs have not been analysed. This paper provides a complete systematic summary of the EXTs for all the TN/ATN, ERS and EOS platforms. It also offers convenient analytical fits for the NOAA platforms, for useful insight into the mechanisms of their EXT evolution and easy practical use. The fit equations are accurate enough to reconstruct the historical EXT data for different NOAA platforms, and predict their future evolution.

2. Orbital configuration and Equator Crossing Time (EXT)

NOAA strives to keep at least two platforms in space at all times by launching new satellites to replace the aged ones. The two orbits have been carefully chosen to take four measurements a day approximately equidistant in time, at the same local solar time (LT) day after day, to provide for consistent scene illumination (in the solar reflectance bands) or segment of diurnal cycle (in the Earth emission bands). One platform is termed *morning* and the other *afternoon*, with orbital planes about 90° (six hours) apart along the approximate north–south axis. The afternoon satellites are launched in an ascending (northbound) orbit, with an EXT (η) of $\sim$1500 (TIROS-N), $\sim$1430 (NOAA-7, -9), $\sim$1330 (NOAA-11, -14), or $\sim$1400 (NOAA-16). These orbits descend back from north to south on the dark side of the Earth at (η-12)$\sim$0300, 0230, 0130, or 0200, respectively. The morning satellites descend from north to south at $\eta\sim$0730, and ascend from south to north in the local evening, at ($\eta+12$)$\sim$1930. NOAA-17 is the first mid-morning satellite, with descending (southbound) node passing at $\eta\sim$1000, and ascending (northbound) node occurring at ($\eta+12$)$\sim$2200. Note that the definitions of the morning and afternoon platforms, widely used in the community, should be considered a mere convention, to differentiate between the two types of orbit. They may appear confusing to a fresh user of NOAA data. In particular, both platforms have AM and PM passes (unlike their names may suggest). Furthermore, the AM pass of a morning platform occurs while on a descending part of the orbit, whereas the PM

pass of an afternoon platform is on an ascending part. In fact, both platforms ascend from south to north in the local afternoon ($\eta \sim 1330$ and 1930), and descend back from north to south during the local morning ($\eta \sim 0130$ and 0730). Additionally, the above EXTs are but target overpass times at launch, whereas the actual EXTs systematically change during the satellite's lifetime as discussed below. Whatever the evolution of the EXT during the lifetime of a platform, its morning or afternoon attribute designated at launch remains unchanged.

The ERS and EOS platforms are designed to allow correction of the orbit during the satellite's lifetime, and therefore their EXTs are expected to be more stable than for NOAA satellites.

3. Data

The NOAA keeps records of the TN/ATN ephemeris for the active (operational) phase of each platform only. The Brouwer-Lyddane orbit prediction package (Kidwell 1998, Goodrum *et al.* 2003) is used to calculate, for each orbit, the longitude of the point at which the satellite crosses the plane of the Equator in a south to north direction (this point is called the ascending node, *AN*), λ_{AN} (°) and the respective *AN* time, T_{AN} (h) (in Coordinated Universal Time, UTC), from which the local EXT, η (h), is calculated as $\eta = T_{AN} - \lambda_{AN}/15^\circ$ (e.g. Duffett-Smith 1988). Historical NOAA ephemeris files are available in three different formats with a non-uniform quality (the number of non-smooth data/outliers progressively increasing towards earlier platforms) at ftp://ftp2.ncdc.noaa.gov/pub/data/orbit/crossing/ and current data are available at http://www.osdpd.noaa.gov/PSB/PPP/NAVIGATION/navpage.html. Useful information about NOAA platforms (launch dates, operational periods, etc.) can be found at http://www.earth.nasa.gov/history/noaa/ and http://www.oso.noaa.gov/poesstatus/.

The US Space Command (USSPACECOM; formerly the North American Aerospace Defense Command, NORAD), which is in charge of monitoring the motion of all orbital targets near the Earth, produces the two-line-element (TLE) dataset. The TLE data are available from various Internet sites for the full lifetime period of many meteorological platforms, including NOAA, ERS and EOS. In this study, data from http://celestrak.com are used from 1980 onwards, which are available in a consistent format and exhibit few outliers. Note that in contrast to NOAA data, the TLE calculations are run on a per need basis rather than for every orbit. The reference times (epoch) at which the TLE data are reported were chosen to be the same T_{AN} as in the NOAA data (this fact is essential as it greatly simplifies the calculation of the EXT from the TLE). Among other parameters, the TLE files report the right ascension of the *AN* of a platform, Ω (defined as the angle between the vernal equinox and the *AN*). The longitude of the equator crossing is obtained by subtracting from Ω the Greenwich mean sidereal time, Θ (expressed as the angle between the vernal equinox and the Greenwich meridian): $\lambda_{AN} = \Omega - \Theta$, and the local standard time of the equator crossing is subsequently calculated as $\eta = T_{AN} - \lambda_{AN}/15^\circ$. More details are found for example in Duffett-Smith (1988).

In what follows, the TLE and NOAA data are compared for the NOAA platforms, and show excellent agreement. For the ERS and EOS platforms, the NOAA data are not available and therefore the TLE data are used.

4. Results

Figures 1 and 2 plot the EXTs for the seven afternoon (ascending node; subtract 12 h for the descending node) and six morning (descending node; add 12 h for the

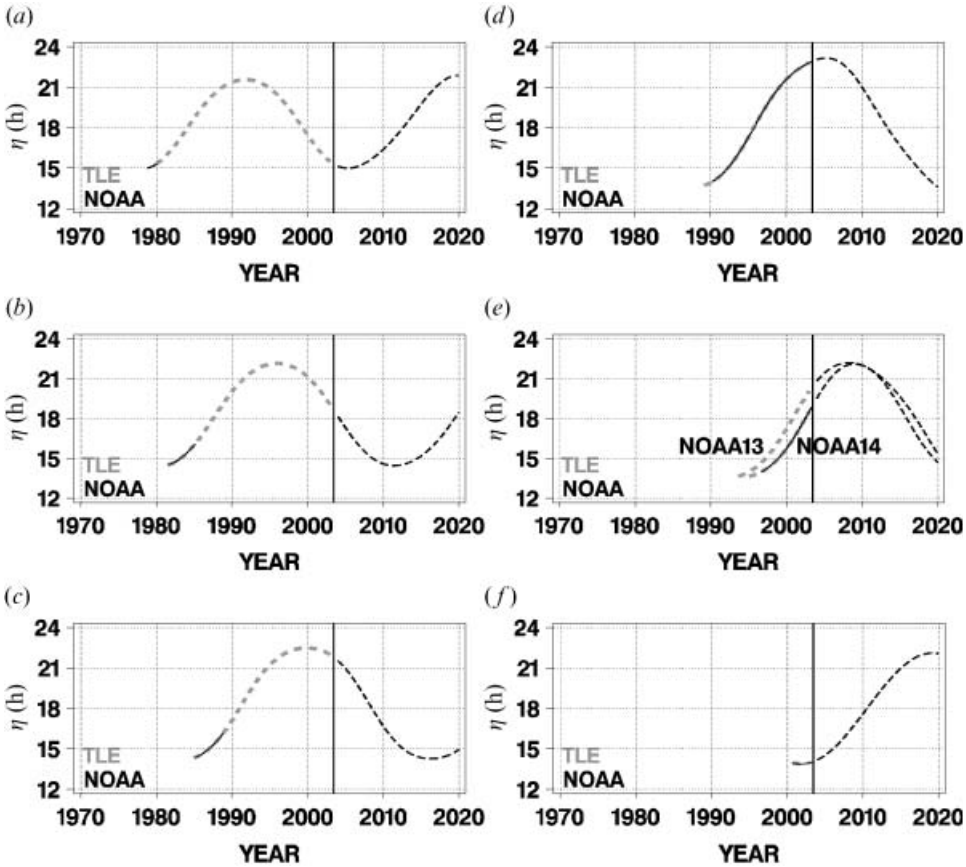

Figure 1. Local Equator crossing time, EXT (ascending/northbound node), η (h), for the seven NOAA afternoon platforms. (*a*) TIROS-N, (*b*) NOAA-7/C, (*c*) NOAA-9/F, (*d*) NOAA-11/H, (*e*) NOAA-13/I and -14/J, (*f*) NOAA-16/L. (Note that NOAA-13 experienced power failure shortly after launch, and therefore was replaced by NOAA-14. The two 'twin' platforms are shown in one panel (*e*).) Dashed grey: the two-line element (TLE) data. Solid black: the NOAA data. Dashed black: extrapolation of the EXT based on fit equation (1) and data in table 1. Solid vertical lines separate the past EXTs prior to 2003, and their future projection beyond 2004.

ascending node) platforms, respectively. (Note that NOAA-13 experienced a power loss due to a circuit failure shortly after launch, and NOAA-14 was launched to replace it. These 'twin' platforms are combined in figure 1(*e*).) At the time of writing, all 13 TN/ATN platforms continue to be in orbit, albeit some of them stopped sending data to Earth years ago. The TLE data are available for a full life cycle of each platform, with the exception of TIROS-N, which was launched in October 1978. Here, NOAA data are available through January 1980, and TLE data from January 1980 onwards. As mentioned above, the NOAA data cover only the active fraction of a platform's life (see e.g. the left panels of figures 1 and 2). In the overlapping periods, the two EXTs (derived from the TLE and NOAA data) agree within a few seconds.

The afternoon platforms are typically launched with $\eta \sim 1400$, and begin drifting to a later afternoon immediately thereafter. Their EXTs reach a maximum of $\eta_{\max} \sim 2200$ after ~ 15 years in orbit, and then drift back to a $\eta_{\min} \sim 1400$ in the next

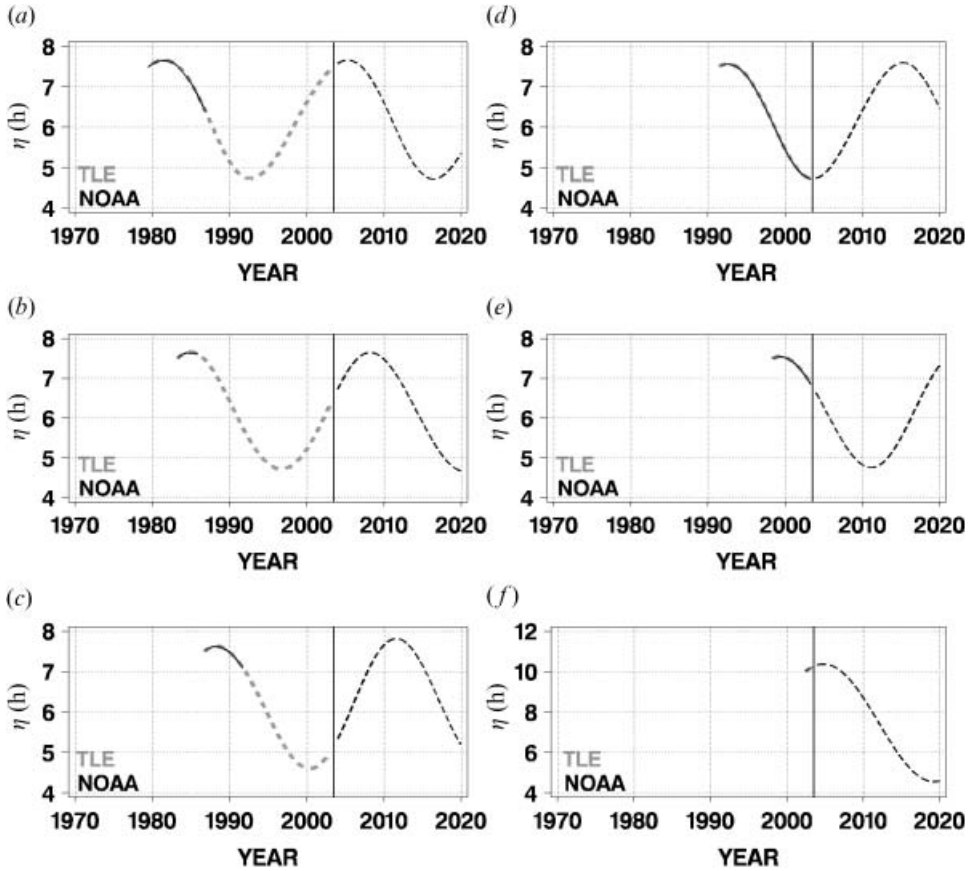

Figure 2. Same as figure 1 but for the six morning NOAA platforms (descending/southbound node). (*a*) NOAA-6/A (*b*) NOAA-8/E, (*c*) NOAA-10/G, (*d*) NOAA-12/D, (*e*) NOAA-15/K, (*f*) NOAA-17/M.

15 years or so. The NOAA-16 is slightly different as its orbit was 'stabilized', i.e. phased in such a way that its EXT first made a $\sim$1.5-year long motion towards noon, before it started drifting towards later times in the same way as the previous afternoon platforms did. The idea of re-phasing the afternoon orbit has been a subject of discussion in the remote sensing community for a long time (see e.g. Price 1991). However, the risk for a platform to drift back in time too far, due to imprecise initial orbital conditions (and possibly ruin the power system due to the increased angle of incidence of the Sun on the solar panels, Price 1991), was not minimized until very recently, when the launching rockets became accurate enough to provide highly predictable orbits. For all afternoon platforms, the range is $\Delta\eta = \eta_{\max} - \eta_{\min} \sim 8$ h, and centred about $\eta \sim 0600/1800$ (descending/ascending orbits, respectively).

The morning orbits all appear to be 'stabilized'. Launched around $\eta \sim 0730$, they first briefly drift forwards in time, before starting drifting back to $\eta \sim 0430$ and then return to the $\eta \sim 0730$ again. The full cycle takes about $T \sim 24$ years, and the range is $\Delta\eta = \eta_{\max} - \eta_{\min} \sim 3$ h centred about 0600/1800 (descending/ascending orbits, respectively).

The NOAA-17/M was put into an unusual mid-morning orbit with an EXT of

$\eta \sim 1000$ (southbound/descending node). Its full period is $T \sim 28$ years, and the range $\Delta\eta \sim 6$h centred about 0730/1930 (see the next section for an explanation on how its T and $\Delta\eta$ were determined). The NOAA-17 'average' time is thus shifted with respect to both afternoon and morning platforms by 1 h 30 min, and its range $\Delta\eta \sim 6$h falls between the morning ($\Delta\eta \sim 3$ h) and afternoon ($\Delta\eta \sim 8$ h) values.

The EXTs of the ERS (ERS1, ERS2, Envisat; all AM) and EOS (Terra, AM; and Aqua, PM) platforms are shown in figure 3, along with the EXTs for NOAA-16 and -17. The ERS1 and ERS2 maintain their EXTs of $\eta \sim 1030$ within a few minutes, except after the ERS1 was deactivated in March 2000, after which time its EXT began to evolve 'naturally'. In the first two years of its life, the Terra crossed the equator anywhere between $\eta \sim 1031$ and $\eta \sim 1045$. In 2002, a more stable period with $\eta \sim 1031$ commenced. The Envisat crosses the equator at $\eta \sim 1000$, well within a few seconds, and NOAA-17 drifted from $\eta \sim 1000$ at launch to $\eta \sim 1009$ by the end of 2002. The Aqua overflies the equator with η from ~ 1333 to ~ 1335, whereas NOAA-16 launched with $\eta \sim 1358$ had first drifted back in time to $\eta_{\min} \sim 1353$ but returned to the original EXT by the end of 2002.

5. Fitting NOAA EXTs and predicting their future evolution

Approximating time series of the historical EXT with simple analytical functions is insightful into their phenomenology, and useful to represent them succinctly and to predict future evolution. To choose an appropriate form of the fit equation, recall that for a given orbital period, the local EXT of a satellite is determined by the position of its orbital plane in space relative to the direction of the Sun, measured by the right ascension of the ascending node, Ω. The orbital plane is moving, due primarily to gravitational perturbations. Kaula (2000) provides analytical expressions for the rate of change in Ω due to the secular (linearly proportional with time) and periodic perturbations caused by the non-spherical gravitational field of the Earth. Following Kaula's method and integrating the Lagrange equations (equation (3.38) in Kaula 2000) with the disturbing function (equation (3.70) in Kaula 2000) and assuming that the longitude of the ascending node, the argument of perigee and the mean anomaly are all linear functions of time, and the remaining three orbital elements (the semi-major axis,

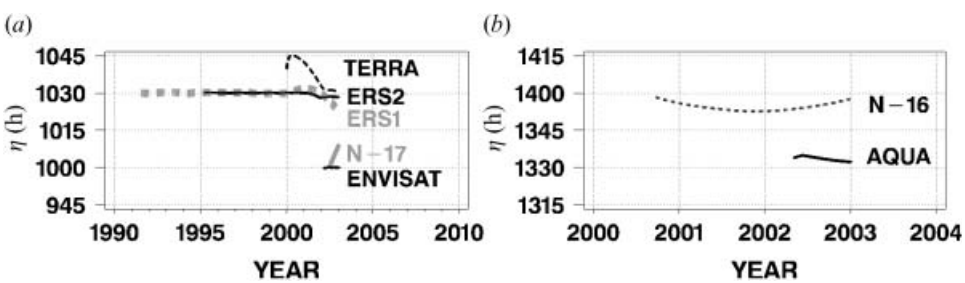

Figure 3. Same as in figure 1 for the (*a*) AM (descending/southbound node) and (*b*) PM (ascending/northbound node) ERS and EOS platforms. EXTs for the mid-morning NOAA-17 and afternoon NOAA-16 platforms are duplicated from panel (*f*) of figures 2 and 1, respectively, for easy comparison.

eccentricity and inclination) are constant, one can write the change $\delta\Omega$ as:

$$\delta\Omega = A(t-t_o) + \sum_{l=1}^{\infty} \{B_l \cos[p_l(t-t_o)+q_l] + C_l \sin[p_l(t-t_o)+q_l]\} \tag{1}$$

Here t is the time elapsed since a chosen reference time t_0, and the constants A, B_l, C_l, p_l, and q_l are functions of the orbital elements.

Note that the other astronomical objects in the solar system (chiefly, the Sun itself) affect the EXT perturbations as well. Their combined effect can still be described in a form of equation (1), but with a different set of parameters.

The orbits of sun-synchronous satellites are designed in such a way that the first (secular) term in $\delta\Omega$, the dominant part of which is due to the equatorial bulge of the Earth, matches the average rate of the Sun's motion projected on the equator: $A \approx 360°/365.25$ days. With respect to this rotating orbital plane, the changes exhibited in the EXT are then represented by the second (periodic) term. We have used this periodic term to guide us in the construction of the function for the fitting. Equation (1) suggests that this term is expressed as an infinite series of sums of cosine and sine functions, with the same frequency and phase for a given index l. To restrict the number of parameters needed in the fit, we replace the infinite series with a sum of a constant and one or two harmonic terms, H_1 and H_2, with different frequencies and phases and arrive at the expression

$$\eta = \eta_o + \alpha_1 \times \sin[\omega_1 \times (\mathrm{JD} - \mathrm{JD}_o) + \phi_1] + \alpha_2 \times \sin[\omega_2 \times (\mathrm{JD} - \mathrm{JD}_o) + \phi_2] \tag{2}$$

that can be viewed as a formal mathematical approximation of a periodic function with one or two Fourier terms. A secular term similar to the $A(t-t_o)$ term in equation (1) representing the residual of the linear drift in the EXT with time was also tested in equation (2), but was found to be statistically insignificant (indicating highly accurate sun-synchronization of the NOAA orbits) and therefore not included. In equation (2), the η_o has a meaning of an average EXT, around which the actual EXT oscillates; the α_i, ω_i, and ϕ_i are the amplitude, frequency, and phase of the respective harmonics ($i = 1,2$), and the JD is the Julian Day (an algorithm for calculating JD is available e.g. from Duffett-Smith 1988); JD_o is the first JD, for which the TLE data were available for a platform (note that it should not be confused with the launch date).

The JD_o and the fit parameters for the afternoon and morning platforms are summarized in tables 1 and 2. The rmse of approximating the historical EXTs with the fit equations, σ_η, is always less than 30 s. Figure 4 additionally plots the residual of the fit for the six early platforms, with the largest rmse. It suggests an excellent agreement between the TLE- and NOAA-derived EXTs. The residuals never exceed

Table 1. Fit parameters in equation (2) for different afternoon NOAA platforms.

	JD_o	η_o (h)	α_1 (h)	ω_1 (JD^{-1})	ϕ_1 (rad)	α_2 (h)	ω_2 (JD^{-1})	ϕ_2 (rad)	RMSE, σ_η (s)
TIROS-N	2444242	18.350	3.367	6.093e–4	5.247	0.150	1.551e–3	4.438	11
NOAA-07	2444779	18.311	3.972	5.419e–4	5.008	0.140	1.511e–3	3.183	21
NOAA-09	2446047	18.367	4.312	5.160e–4	5.064	0.207	1.506e–3	2.969	25
NOAA-11	2447583	18.258	4.935	4.989e–4	5.036	0.164	1.754e–3	2.244	7
NOAA-13	2449209	17.913	4.410	5.603e–4	4.841	0.122	1.811e–3	1.220	3
NOAA-14	2449717	17.759	4.348	5.718e–4	4.809	0.224	1.540e–3	1.451	3
NOAA-16	2451809	18.099	4.141	4.955e–4	4.531	0.212	3.129e–4	3.404	3

Table 2. Fit parameters in equation (2) for different morning NOAA platforms. *NOAA-17 is a mid-morning satellite and therefore its fit parameters differ from the other morning platforms.

	JD_o	η_o (h)	α_1 (h)	ω_1 (JD^{-1})	ϕ_1 (rad)	α_2 (h)	ω_2 (JD^{-1})	ϕ_2 (rad)	RMSE, σ_η (s)
NOAA-06	2444242	6.226	1.458	7.268e–4	1.244	0.080	1.443e–3	5.267	29
NOAA-08	2445422	6.156	1.470	7.310e–4	1.134	0.037	1.650e–3	0.092	7
NOAA-10	2446691	6.176	1.543	7.320e–4	1.159	0.103	1.146e–3	4.123	7
NOAA-12	2448391	6.178	1.421	7.613e–4	1.272	0.041	1.637e–3	4.509	3
NOAA-15	2450947	6.169	1.399	7.507e–4	1.260	0.040	1.356e–3	3.404	2
NOAA-17*	2452450	7.489	2.810	6.000e–4	1.040	0.130	3.267e–4	3.324	1

2 min, and could be further reduced if needed, by adding a third harmonic in equation (2). Using only one harmonic in place of two leads to a less accurate fit

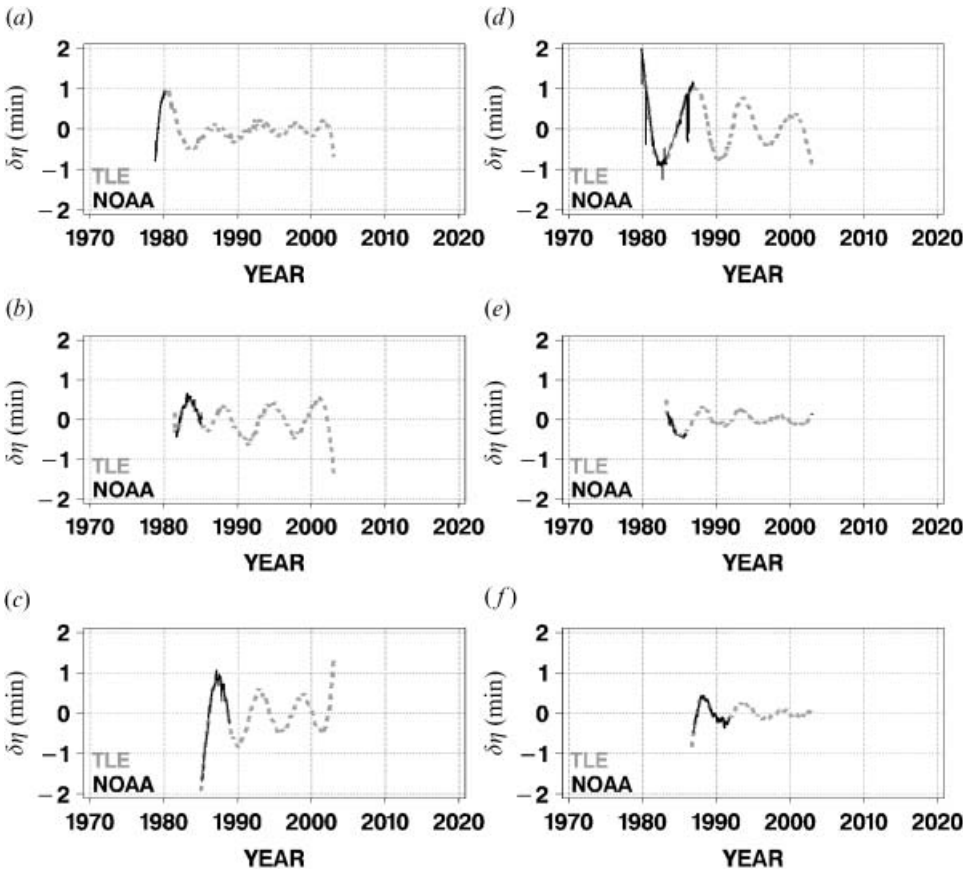

Figure 4. EXT fit error with equation (2) using fit parameters listed in tables 1 and 2, $\delta\eta$ (min), for the six early NOAA platforms with largest approximation errors (see e.g. the last column in tables 1 and 2). (*a*) TIROS-N, (*b*) NOAA-7/C, (*c*) NOAA-9/F, (*d*) NOAA-6/A, (*e*) NOAA-8/E, (*f*) NOAA-10/G. Dashed grey: the two-line element (TLE) data. Solid black: the NOAA data.

(error increases by a factor of 3–4). It is thus concluded that the accuracy of the above three-term expression is sufficient for our purpose.

Note that in the calculation of tables 1 and 2, the (real value) JD in equation (2) was specified from the exact UTC of the satellite equator crossing in ascending node, T_{AN}, which is not available to readers. Numerical estimates show that specifying the (integer value) JD for a centre of a day leads to a worst-case error in the EXT of up to a few seconds, which is typically smaller compared to the fit error and therefore not critical for practical use of equation (2). For example, the EXT for TIROS-N on midday (UTC = 1200) 25 November 1986 (JD = 2446760) is calculated using equation (2) and data in table 1 as $\eta = 20.091$ h. The TLE result for the orbit passing at UTC ~ 0327 on that day is $\eta = 20.09157$ h, a ~ 2 s difference from the predicted value.

In equation (2), η_o is the average EXT. It ranges from $\eta_o \sim 1745$ to $\eta_o \sim 1820$ for the afternoon platforms (ascending node), and from $\eta_o \sim 0610$ to $\eta_o \sim 0615$ for the morning platforms (descending node). This means that if a consistent node is considered, the average EXT is $\eta_o \sim 0600/1800$, and approximately the same for all NOAA platforms except NOAA-17.

The first harmonic (H_1) approximates the EXT shape well. For the afternoon platforms, parameters of H_1 are: $\alpha_1 \sim 3.4$–4.9 h, $\omega_1 \sim (5$–$6) \times 10^{-4}$ (JD^{-1}) (corresponding to a period of $T_1 \sim 28$–35 years), and $\phi_1 \sim 4.5$–5.2. For the morning platforms, parameters of H_1 are: $\alpha_1 \sim 1.4$–1.5 h, $\phi_1 \sim 7.4 \times 10^{-4}$ (JD^{-1}) (corresponding to a period of $T_1 \sim 23$ years), $\varphi_1 \sim 1.1$–1.3. Numerical experiments with a simple model have shown that the empirical periods and amplitudes should be at least an order of magnitude smaller, if the Earth were the only cause of the orbital drift. It is therefore felt that the observed fit parameters and the large differences between the morning and afternoon platforms can be explained only if the effect of the Sun is considered. This is because the secular rate of Ω is very sensitive to variations in the inclination of the orbit, and for sun-synchronous orbits the otherwise small perturbations in the inclination would build up with time (a phenomena known as 'deep resonance' in orbital mechanics) (Vallado 2001). The rate of change in the inclination due to the Sun depends on the desired value of EXT of the satellite (e.g. Price 1991), and thus it is expected that the amplitude of η will be different for the morning (EXT ~ 0730) and the afternoon (EXT ~ 1400) satellites.

The accuracy of the fit is further improved by the second harmonic (H_2). The parameters of the H_2 harmonic for the afternoon platforms are: $\alpha_2 \sim 0.14$–0.22 h, $\omega_2 \sim (1.5$–$1.8) \times 10^{-3}$ (JD^{-1}) (corresponding to a period of $T_2 \sim 9$–11 years), $\phi_2 \sim 1.2$–4.4. For the morning platforms, $\alpha_2 \sim 0.04$–0.10 h, $\omega_2 \sim (1.1$–$1.6) \times 10^{-3}$ (JD^{-1}) (corresponding to a period of $T_2 \sim 11$–16 years), $\phi_2 \sim 0$–5.3.

All fit parameters (except for the phase of H_2) appear well reproducible from one platform to another. Note that frequencies of H_2 for the NOAA-16 and -17 are about five times lower compared to their predecessors. Additionally, the NOAA-17 average EXT $\eta_o \sim 0730/1930$ is dramatically different from all other NOAA platforms.

Future projections (up to 2020) of the EXTs for all NOAA platforms based on the estimated fit equations are also plotted in figures 1 and 2. Predictions are undoubtedly more accurate for the earlier platforms, but are deemed to be good at least qualitatively for the more recent platforms (such as NOAA-16 and -17) as well, being based on the physical equation (2), whose parameters are reproducible for all similar platforms. In particular, the NOAA-16 will be flying at $\eta \sim 1500$ by

2006, at $\eta \sim 1600$ by 2008, and at $\eta \sim 1800$ by 2011. The NOAA-17 EXT will reach its maximum of $\eta_{\max} \sim 1020$ by 2005, then return back to the launch value of $\eta \sim 1000$ by 2007, and subsequently decline to $\eta \sim 0900$ by 2009 and further to $\eta \sim 0800$ by 2011.

6. EXT and local time of observation

When using the EXT as a proxy for the LT of satellite sensor observation, two factors should be considered. First, the LT changes systematically with latitude, due to the Earth rotation and orbit inclination, even for nadir views. Simple geometrical considerations suggest that the local pass time at a latitude φ, $\eta_{A\varphi}$ (h), is represented for the ascending and descending branches as

$$\eta_{A\varphi} = \eta_{Ao} + \frac{\arcsin\left(\frac{\tan(\varphi)}{\tan(i)}\right)}{15^\circ}; \quad \eta_{D\varphi} = \eta_{Do} - \frac{\arcsin\left(\frac{\tan(\varphi)}{\tan(i)}\right)}{15^\circ} \tag{3}$$

respectively where i is the orbital inclination which also changes systematically over the lifetime of a platform. For NOAA platforms, a representative number of $i \sim 99.0^\circ \pm 0.4$ can be used. Note that $\tan(i) < 0$, and therefore on an ascending pass, $\eta_{A\varphi} < \eta_{Ao}$ ($\eta_{A\varphi} > \eta_{Ao}$) to the north (south) of the Equator, whereas on a descending pass, $\eta_{D\varphi} > \eta_{Do}$ ($\eta_{D\varphi} < \eta_{Do}$). In particular, the min/max latitude can be estimated from equation (3) as a point at which $\eta_{A\varphi} = \eta_{D\varphi}$. Recalling $\eta_{Ao} = \eta_{Do} + 12$, one obtains $\varphi_{\max}/\varphi_{\min} = \pm(180^\circ\text{-}i) \sim \pm 81^\circ$. This latitude is reached six hours from both η_{Ao} and η_{Do}, i.e. exactly between the two EXTs.

Equation (3) can be used for a non-scanning radiometer onboard NOAA such as the SBUV instrument. Other radiometers onboard NOAA platforms (AVHRR, HIRS, MSU and SSU) scan cross-track, and therefore may 'look' more than a thousand kilometres off nadir. Calculation of the local observation time from these sensors requires additional correction for the scan effect.

7. Conclusion

The systematic changes of the local observation time during the life cycle of a platform, and between different platforms, are significant and should be accounted for when using multi-year time series of satellite products in long-term monitoring/climate analyses. The current paper systemizes the available information on the EXT for the sun-synchronous weather and climate platforms, and represents it succinctly with simple analytical formulae to facilitate calculation of the past EXTs for the NOAA platforms, and prediction of their future evolution. One observation which clearly emerges from our analyses is that the term 'orbital degradation' commonly used in literature on NOAA satellites should be avoided, and a more appropriate term such as 'orbital evolution' should be used instead.

Acknowledgements

Thanks go to Konstantin Vinnikov (University of Maryland, USA), Dan Tarpley, Jerry Sullivan, Felix Kogan, Mike Weinreb, Shobha Kondragunta, Larry Flynn, Jim Miller, Changyong Cao, Nick Nalli, Paul Menzel, Yan Ming Wang, Alex Kidd, and Mike Simpson (NOAA, USA) for helpful discussions and advice, and help with the NOAA equator crossing time data. This work was funded under the Integrated Program Office (NOAA/NASA/DOD), NASA EOS/CERES (NASA contract L-90987C), NOAA/NESDIS Ocean Remote Sensing and Polar Satellites Programs, and Joint Center for Satellite Data Assimilation. We are thankful to

Steve Mango (IPO), Bruce Wielicki (NASA/LaRC), Al Strong, Bill Pichel, Mike Mignogno, Tom Schott, and Fuzhong Weng (NOAA/NESDIS) for their support and encouragement. The views, opinions, and findings contained in this report are those of the authors and should not be construed as an official National Oceanic and Atmospheric Administration or US Government position, policy, or decision.

References

BATES, J., WU, X., and JACKSON, D., 1996, Interannual variability of upper-troposphere water vapor band brightness temperature. *Journal of Climate*, **9**, 427–438.

BREST, C., ROSSOW, W., and ROITER, M., 1997, Update of radiance calibrations for ISCCP. *Journal of Atmospheric and Oceanic Technology*, **14**, 1091–1109.

BROWNSCOMBE, J., NASH, J., VAUGHAN, G., and ROGERS, C., 1985, Solar tides in the middle atmosphere I. Description of satellite observations and comparison with theoretical calculations at equinox. *Quarterly Journal of the Royal Meteorological Society*, **111**, 677–689.

CAO, C., SULLIVAN, J., MATURI, E., and SAPPER, J., 2002, The effect of orbit drift on the radiometric calibration of the 3.7 μm channel of the AVHRR onboard NOAA-14 and its impact on night-time sea surface temperature retrievals. *International Journal of Remote Sensing*, **25**, 975–986.

CHRISTY, J., SPENCER, R., NORRIS, W., and BRASWELL, W., 2003, Error estimates of version 5.0 of MSU-AMSU bulk atmospheric temperatures. *Journal of Atmospheric and Oceanic Technology*, **20**, 613–629.

CRACKNELL, A. P., 1997, *The Advanced Very High Resolution Radiometer* (London: Taylor & Francis).

CRACKNELL, A. P. (editor), 2001, *Remote Sensing and Climate Change* (Chichester, UK: Praxis Publishing).

DUFFETT-SMITH, P., 1988, *Practical Astronomy with your Calculator*, 3rd edn (New York: Cambridge University Press).

FLYNN, L., KONDRAGUNTA, S., HORVATH, K., and BEACH, E., 2000, Internal validation of SBUV/2 ozone vertical profile dataset. *Proceedings of the Quadrennial Ozone Symposium, Hokkaido University, Sapporo, Japan 3–8 July 2000*, pp. 75–76.

GOODRUM, G., KIDWELL, K., and WINSTON, W. (editors), 2003, NOAA–KLM User's Guide. US Department of Commerce, NOAA/NESDIS. Available from National Climatic Data Center, 151 Patton Ave, Rm.120, Asheville, NC 28801-5001, USA, http://www2.ncdc.noaa.gov/docs/klm/index.htm.

GUTMAN, 1999 a, On the monitoring of land surface temperatures with the NOAA/AVHRR: removing the effect of satellite orbit drift. *International Journal of Remote Sensing*, **20**, 3407–3413.

GUTMAN, 1999 b, On the use of long-term global data of land reflectances and vegetation indices derived from AVHRR. *Journal of Geophysical Research*, **104**, 6241–6255.

GUTMAN, G., and IGNATOV, A., 1995, Global land monitoring from AVHRR: potential and limitations. *International Journal of Remote Sensing*, **16**, 2301–2309.

JACKSON, D., and BATES, J., 2001, Climate analysis with the 21-year HIRS Pathfinder radiance clear-sky data set. *Proceedings of the 11th Conference on Satellite Meteorology & Oceanography, Madison, Wisconsin, 15–18 October 2001*.

KAULA, W., 2000, *Theory of Satellite Geodesy: Applications of satellites to geodesy*, reprint edn (New York: Dover).

KIDDER, S., and VONDER HAAR, T., 1995, *Satellite Meteorology: An Introduction* (New York: Academic Press).

KIDWELL, K. (editor), 1998, NOAA Polar Orbiter Data User's Guide (TIROS–N, NOAA-6, -7, -8, -9, -10, -11, -12, -13, and -14. US Department of Commerce, NOAA/NESDIS, 394 pp. Available from National Climatic Data Center, 151 Patton Ave, Rm.120, Asheville, NC 28801–5001, USA, http://www2.ncdc.noaa.gov/docs/podug/index.htm.

KOGAN, F., and ZHU, X., 2001, Evolution of long-term errors in NDVI time series: 1985–1999. *Advances in Space Research*, **28**, 149–153.

MEARS, C., SHABEL, M., and WENTZ, F., 2003, A reanalysis of the MSU channel 2 tropospheric temperature record. *Journal of Climate*, **16**, 3650–3664.

MENZEL, P., WYLIE, D., JACKSON, D., and BATES, J., 2002, HIRS observations of clouds

since 1978. *Proceedings of the Conference on Applications with Weather Satellites at the SPIE 3rd International Asia-Pacific Environmental Remote Sensing Symposium, Hangzhou, China, 23–27 October 2002*, SPIE Proc. Vol. 4892, pp. 391–397.

MILLER, A., NAGATANI, R., FLYNN, L., KONDRAGUNTA, S., and BEACH, E., STOLARSKI, R., MCPETERS, R., BHARTIA, P. K., and DELAND, M., 2002, A cohesive total ozone data set from SBUV/2 satellite system. *Journal of Geophysical Research*, **107**, 4701.

PRICE, J., 1991, Timing of NOAA afternoon passes. *International Journal of Remote Sensing*, **12**, 193–198.

PRIVETTE, J., FOWLER, C., WICK, G., BALDWIN, D., and EMERY, W., 1995, Effects of orbital drift on AVHRR products: normalized difference vegetation index and sea surface temperature. *Remote Sensing of Environment*, **53**, 164–171.

RAO, P. K., HOLMES, S. J., ANDERSON, R. K., WINSTON, J. S., and LEHR, P. E., editors, 1990, *Weather Satellites: Systems, Data and Environmental Applications* (Boston, MA: American Meteorological Society).

REYNOLDS, R., and GENTEMANN, C., 2004, Impact of TRMM SSTs on a climate-scale SST analysis. *Journal of Climate*, **17**, 2314–2328.

STOWE, L., JACOBOWITZ, H., OHRING, G., KNAPP, K., and NALLI, N., 2002, The AVHRR Pathfinder Atmosphere (PATMOS) climate data set: initial analyses and evaluations. *Journal of Climate*, **15**, 1243–1260.

VALLADO, A. D., 2001, *Fundamentals of Astrodynamics and Applications*, 2nd edn, Space Technology Laboratory, Vol. 12 (Dordrecht: Kluwer Academic).

VINNIKOV, K., and GRODY, N., 2003, Global warming trend in satellite observed mean troposphere temperature. *Science*, **302**, 269–272.

WALISER, D., and ZHOU, W., 1997, Removing satellite equatorial crossing time biases from the OLR and HRC datasets. *Journal of Climate*, **10**, 2125–2146.